Appendix: PIV data

Supplemental material for the manuscript:
"Simplified model for helical vortex dynamics in the wake of an asymmetric rotor"
by Aliza Abraham, Andrés Castillo-Castellanos, and Thomas Leweke

A description of the methods and a subset of the data obtained using particle image velocimetry (PIV) are presented in this appendix.

The raw PIV images were obtained by seeding the water channel with 10 µm-diameter silver-coated hollow glass spheres and illuminating a cross-section of the test section below the rotor using a double-pulsed Nd:YAG laser with a 532 nm wavelength. The laser pulses had a spacing of 2 ms and were synchronized with the frame capture rate of the camera at 4.5 Hz. The camera and laser were both synchronized with the rotor rotation such that an image pair was captured every 4/3 rotation. Using this timing, each set of three image pairs captured the tip vortices shed from all three blades. For each image sequence, 900 pairs were collected, leading to 300 pairs per blade. This process was repeated using 12 different time delays between the blade passage and the frame capture, such that image pairs were obtained at every 10° of rotor rotation, capturing the tip vortices at different stages of their evolution. With each sequence including images from all three blades, a total of 36 phases of rotor rotation were obtained for the baseline symmetric rotor. Note that the baseline rotor still had a small residual asymmetry, where the tip position of blade 0 was offset by $(x_0/R, y_0/R) = (1.13, 0.24) \times 10^{-3}$ from that of blade 2, and that of blade 0 was $(x_1/R, y_1/R) = (0.04, 0.95) \times 10^{-3}$ away from that of blade 2.

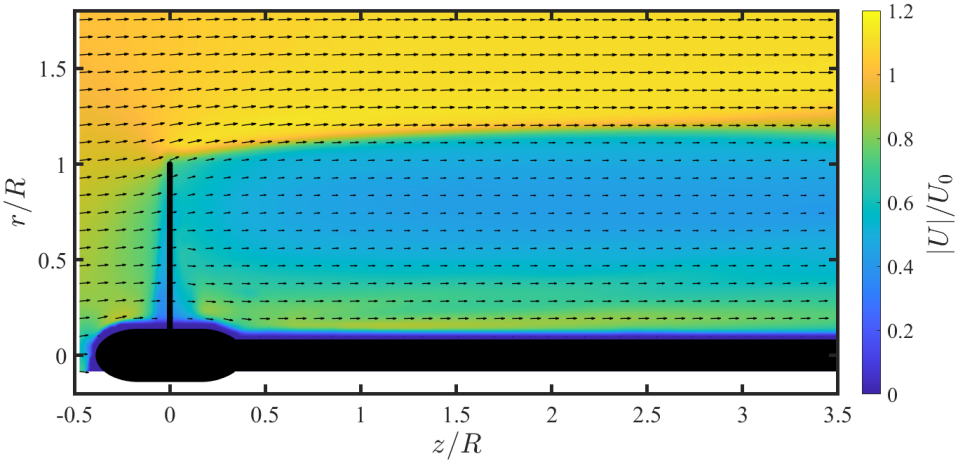

Figure 1: Mean velocity field for the baseline symmetric rotor. The color represents the magnitude of the velocity, and the vectors indicate the direction. The vector spacing is decreased by a factor of 10 from the real resolution for readibility.

The raw images (3388 × 1712 pixels) were processed in MATLAB using an in-house PIV code called DPIV-Soft 2019. Two passes were used, the first with a 64 × 64 pixel correlation window and

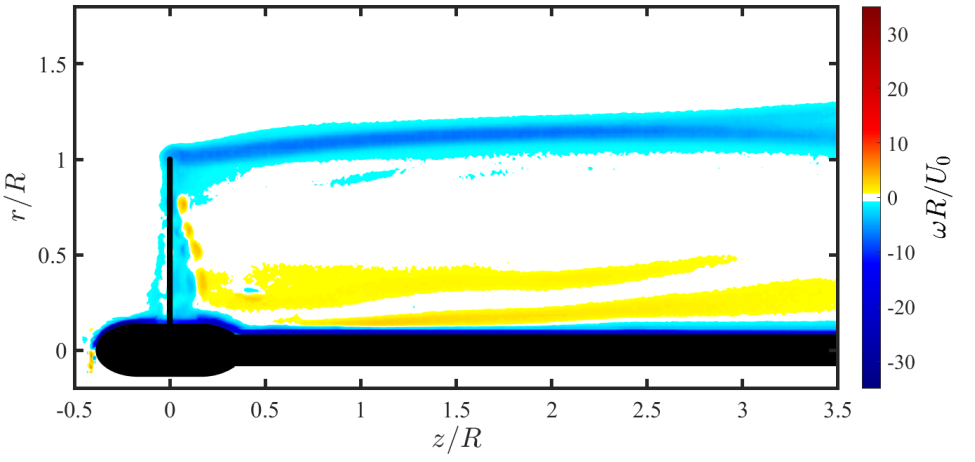

Figure 2: Mean out-of-plane vorticity field for the baseline symmetric rotor.

the second with a 32×32 pixel window, both with 50% overlap. The average of all 36 phases were used to compute the mean velocity and vorticity fields shown in Figures 1 and 2, respectively.

For the vortex properties (i.e., circulation, helical pitch) discussed in the main text, phase-locked average vorticity fields were used, such as the example shown in Figure 3. Using each phase-averaged vorticity field, the center of each tip vortex was manually selected. The z-position of these vortex centers were used to calculate the vortex spacing, h/R (Figure 4). An asymptotic equation was fit to the mean h/R values at each z/R, and the value of the asymptote was used for the $h = 4.72 \pm 0.09$ cm value reported in the manuscript. As is evident from Figure 4, this value is approached very quickly, within $z = 1R$. Similarly, the r-position of the vortex centers were used to calculate the wake expansion, R_w/R (Figure 5). Once again, the mean R_w/R value was calculated for each z/R, and an asymptotic fit was applied. These fitted values were used for R_w in the manuscript.

The phase-locked vorticity fields were also used to calculate the circulation of the vortices shed from each of the three blades. Circulation was calculated as the line integral of velocity around a circle of radius $h/3$, centered at the manually-selected vortex center (Figure 3). As seen in Figure 6, the circulation of all three vortices starts to decrease around $z/R \approx 1$, attributed to the vorticity from the vortex sheets within the wake entering the circles used to calculate the circulation. Therefore, the circulation values of each vortex are computed as the mean of the circulation between $z/R = 0$ and $z/R = 1$. Some variability ($\sim 3\%$) in the values of the vortices shed from the three blades is observed, likely due to small, unavoidable differences in their geometry or alignment. The mean circulation of the three vortices is used for the baseline symmetric rotor in the manuscript: $\Gamma = 165 \pm 3$ cm^2/s. The same process was used to calculate the circulation of the tip vortices for all asymmetric configurations reported in the manuscript, though only 3 phases of rotor rotation were captured rather than 36.

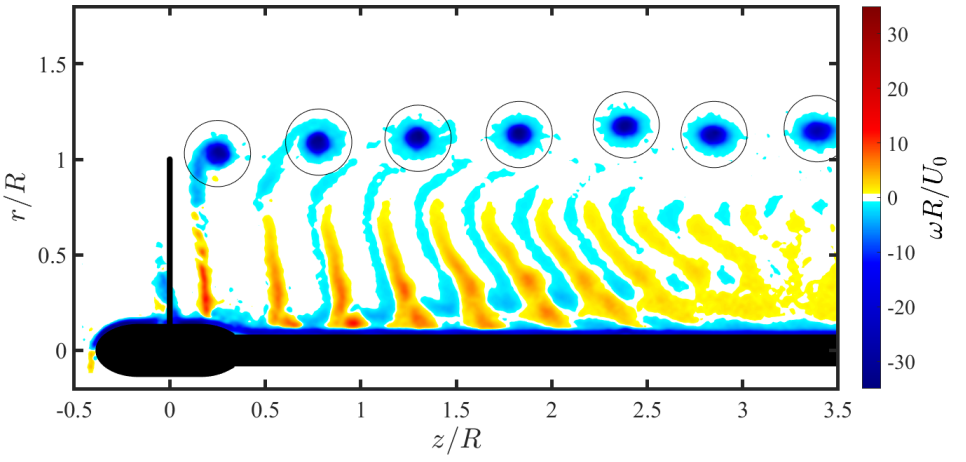

Figure 3: Phase-locked average vorticity field for the baseline symmetric rotor. The vorticity field shown here was captured at the time when the most recently shed tip vortex (from blade 2) was located at $z \sim h/2$, corresponding to a rotor rotation phase of 60°. The black circles indicate the lines used for the computation of tip vortex circulation.

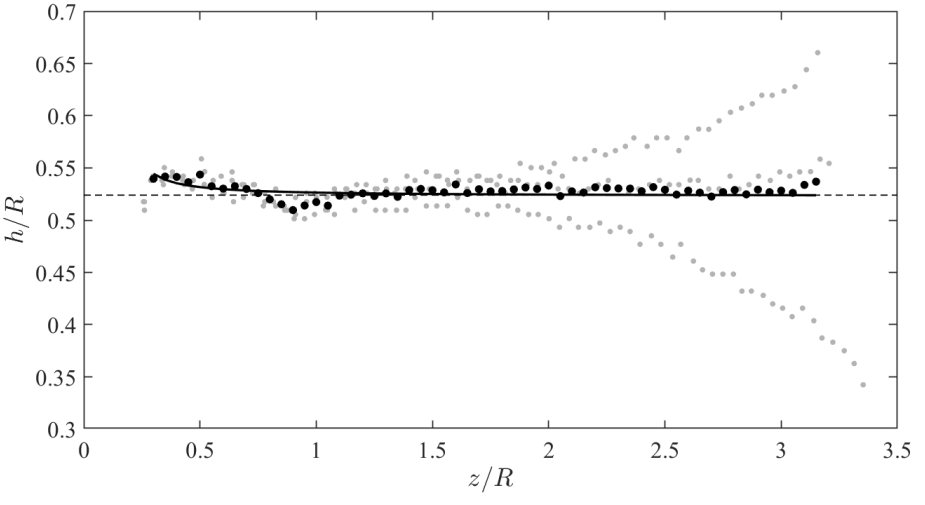

Figure 4: Helical pitch of the tip vortices shed from the baseline symmetric rotor. The gray points represent each measured value of h/R, the black circles are the mean of the measurements, and the solid black line is an asymptotic fit to the mean. The dashed line is drawn at the value of the asymptote. The deviations between the three trajectories are due to the slight asymmetry of the baseline rotor.

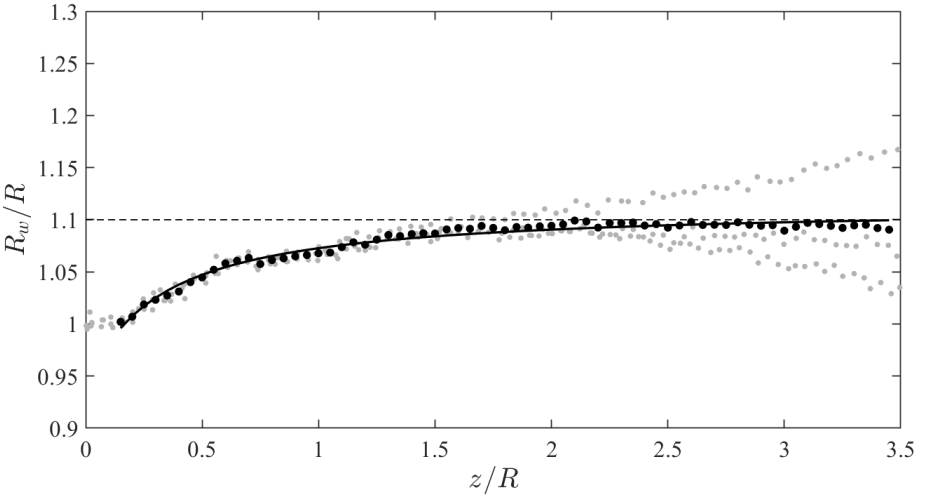

Figure 5: Radius of the wake behind the baseline symmetric rotor, as determined by the radial positions of the tip vortices. The gray points represent each measured value of R_w/R, the black circles are the mean of the measurements, and the solid black line is an asymptotic fit to the mean. The dashed line is drawn at the value of the asymptote. The deviations between the three trajectories are due to the slight asymmetry of the baseline rotor.

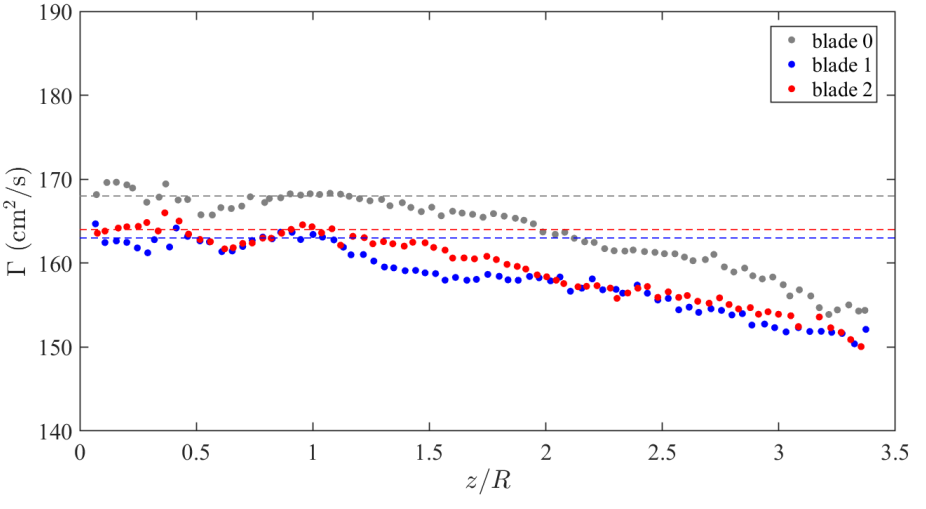

Figure 6: Circulation of the tip vortices shed from each of the three blades of the baseline symmetric rotor. The dashed lines indicate the average values of Γ for $z/R < 1$.